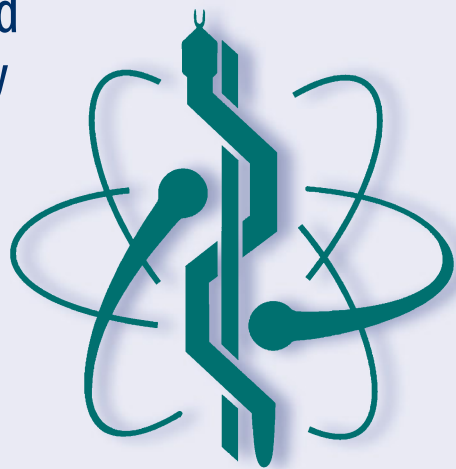


Guangzhi Wang · Dezhong Yao ·
Zhongze Gu · Yi Peng ·
Shanbao Tong · Chengyu Liu *Editors*

12th Asian-Pacific Conference on Medical and Biological Engineering

Proceedings of APCMBE 2023, May 18–21,
2023, Suzhou, China—Volume 2:
Computer-Aided Surgery, Biomechanics,
Health Informatics, and
Computational Biology



Series Editor

Ratko Magjarević, *Faculty of Electrical Engineering and Computing, ZESOI, University of Zagreb, Zagreb, Croatia*

Associate Editors

Piotr Ładyżyński, *Warsaw, Poland*

Fatimah Ibrahim, *Department of Biomedical Engineering, Faculty of Engineering, Universiti Malaya, Kuala Lumpur, Malaysia*

Igor Lackovic, *Faculty of Electrical Engineering and Computing, University of Zagreb, Zagreb, Croatia*

Emilio Sacristan Rock, *Mexico DF, Mexico*

The IFMBE Proceedings Book Series is an official publication of *the International Federation for Medical and Biological Engineering* (IFMBE). The series gathers the proceedings of various international conferences, which are either organized or endorsed by the Federation. Books published in this series report on cutting-edge findings and provide an informative survey on the most challenging topics and advances in the fields of medicine, biology, clinical engineering, and biophysics.

The series aims at disseminating high quality scientific information, encouraging both basic and applied research, and promoting world-wide collaboration between researchers and practitioners in the field of Medical and Biological Engineering.

Topics include, but are not limited to:

- Diagnostic Imaging, Image Processing, Biomedical Signal Processing
- Modeling and Simulation, Biomechanics
- Biomaterials, Cellular and Tissue Engineering
- Information and Communication in Medicine, Telemedicine and e-Health
- Instrumentation and Clinical Engineering
- Surgery, Minimal Invasive Interventions, Endoscopy and Image Guided Therapy
- Audiology, Ophthalmology, Emergency and Dental Medicine Applications
- Radiology, Radiation Oncology and Biological Effects of Radiation
- Drug Delivery and Pharmaceutical Engineering
- Neuroengineering, and Artificial Intelligence in Healthcare

IFMBE proceedings are indexed by SCOPUS, EI Compendex, Japanese Science and Technology Agency (JST), SCImago. They are also submitted for consideration by WoS.


Proposals can be submitted by contacting the Springer responsible editor shown on the series webpage (see “Contacts”), or by getting in touch with the series editor Ratko Magjarevic.


Guangzhi Wang · Dezhong Yao · Zhongze Gu ·
Yi Peng · Shanbao Tong · Chengyu Liu
Editors

12th Asian-Pacific Conference on Medical and Biological Engineering

Proceedings of APCMBE 2023, May 18–21,
2023, Suzhou, China—Volume 2:
Computer-Aided Surgery, Biomechanics,
Health Informatics,
and Computational Biology

Editors


Guangzhi Wang 
Department of Biomedical Engineering
School of Medicine
Tsinghua University
Beijing, China

Dezhong Yao 
School of Life Science and Technology
University of Electronic Science
and Technology
Chengdu, China

Zhongze Gu
State Key Laboratory of Bioelectronics
School of Biological Science and Medical
Engineering
Southeast University
Nanjing, China

Yi Peng
Institute of Basic Medical Sciences
Chinese Academy of Medical Sciences
and Peking Union Medical College
Beijing, China

Shanbao Tong
School of Biomedical Engineering
Shanghai Jiao Tong University
Shanghai, China

Chengyu Liu 
State Key Laboratory of Bioelectronics
School of Instrument Science
and Engineering
Southeast University
Nanjing, China

ISSN 1680-0737

ISSN 1433-9277 (electronic)

IFMBE Proceedings

ISBN 978-3-031-51484-5

ISBN 978-3-031-51485-2 (eBook)

<https://doi.org/10.1007/978-3-031-51485-2>

© The Editor(s) (if applicable) and The Author(s), under exclusive license to Springer Nature Switzerland AG 2024

This work is subject to copyright. All rights are solely and exclusively licensed by the Publisher, whether the whole or part of the material is concerned, specifically the rights of translation, reprinting, reuse of illustrations, recitation, broadcasting, reproduction on microfilms or in any other physical way, and transmission or information storage and retrieval, electronic adaptation, computer software, or by similar or dissimilar methodology now known or hereafter developed.

The use of general descriptive names, registered names, trademarks, service marks, etc. in this publication does not imply, even in the absence of a specific statement, that such names are exempt from the relevant protective laws and regulations and therefore free for general use.

The publisher, the authors, and the editors are safe to assume that the advice and information in this book are believed to be true and accurate at the date of publication. Neither the publisher nor the authors or the editors give a warranty, expressed or implied, with respect to the material contained herein or for any errors or omissions that may have been made. The publisher remains neutral with regard to jurisdictional claims in published maps and institutional affiliations.

This Springer imprint is published by the registered company Springer Nature Switzerland AG
The registered company address is: Gewerbestrasse 11, 6330 Cham, Switzerland

Paper in this product is recyclable.

APCMBE2023 Committees

Presidium

President

Xuetao Cao Chinese Academy of Medical Sciences

Executive President

Shengshou Hu Fuwai Hospital, Chinese Academy of Medical Sciences

Vice Presidents

Jing Cheng Tsinghua University
Hui Chi Medical Information Research Institute of
Chinese Academy of Medical Sciences
Xiaosong Gu Nantong University
Jinxiang Han Shandong First Medical University
Deyu Li Beihang University
Suiren Wan Southeast University
Guangzhi Wang Tsinghua University
Guosheng Wang Henan Tuoren Medical Device Co., Ltd.
Dezhong Yao University of Electronic Science and Technology
of China
Yiwu Zhao Naton Medical Group
Hairong Zheng Shenzhen Institutes of Advanced Technology,
Chinese Academy of Sciences

Secretary-General

Hui Chi Medical Information Research Institute of
Chinese Academy of Medical Sciences

Local Organizing Committee Members

Xin Chen	Shenzhen University
Xun Chen	University of Science and Technology of China
Xiang Dong	Naton Medical Group
Jianzeng Dong	Beijing Anzhen Hospital, Capital Medical University
Qianjin Feng	Southern Medical University
Feng Fu	Air Force Medical University
Xingming Guo	Chongqing University
Gang Huang	Shanghai University of Medicine and Health Sciences
Baohua Ji	Zhejiang University
Linhong Ji	Tsinghua University
Hua Jiang	Zhejiang University
Xieyuan Jiang	Beijing Jishuitan Hospital
Xinquan Jiang	The Ninth People's Affiliated Hospital of Shanghai Jiao Tong University School of Medicine
Yan Kang	Shenzhen Technology University
Xixiong Kang	Beijing Tiantan Hospital, Capital Medical University
Bin Li	Shanghai Sixth People's Hospital Affiliated to Shanghai Jiaotong University
Changying Li	Beijing Aeonmed Co., Ltd.
Tao Li	Tianjin Third Central Hospital
Pengcheng Li	Huazhong University of Science and Technology
Jun Liang	The Second Affiliated Hospital of the Air Force Military Medical University
Peixue Ling	National Glycoengineering Research Center
Gang Liu	Xiamen University
Hui Liu	Chinese Academy of Medical Sciences
Lihua Liu	The Fourth Hospital of Hebei Medical University
Yajun Liu	Beijing Jishuitan Hospital of Capital Medical University
Zhicheng Liu	Capital Medical University
Aili Lu	Tsinghua University
Jiaxin Liu	Chinese Academy of Medical Sciences
Ling Lv	The Fourth School of Clinical Medicine of Nanjing Medical University
Zhenhe Ma	Northeast University
Chenxi Ouyang	Fuwai Hospital, Chinese Academy of Medical Sciences

Zhaolian Ouyang	Medical Information Research Institute of Chinese Academy of Medical Sciences
Yi Peng	Institute of Basic Medical Sciences, Chinese Academy of Medical Sciences
Fang Pu	Beihang University
Xianzheng Sha	China Medical University
Zhu Shen	Sichuan Academy of Medical Sciences/Sichuan Provincial People's Hospital
Guosheng Wang	Henan Tuoren Medical Device Co., Ltd.
Shunren Xia	Hangzhou City University
Guimin Zhang	Lunan Pharmaceutical Group
Songgen Zhang	TINAVI Medical Technologies Co., Ltd.

International Organizing Committee Members

Michael B. Flood	Locus Consulting, Australia
Luming Li	Tsinghua University, China
Hong'en Liao	Tsinghua University, China
Chengyu Liu	Southeast University, China
Jaw-Lin Wang	Taiwan University, Chinese Taipei
Chih-Chung Huang	Cheng Kung University, Chinese Taipei
Min Wang	University of Hong Kong, Hong Kong, SAP
Ming Zhang	The Hong Kong Polytechnic University, Hong Kong, SAP
Ichiro Sakuma	The University of Tokyo, Japan
Keiko Fukuta	Japanese Association for Clinical Engineers, Japan
Mang I. Vai	University of Macau, Macau, SAP
Peng Un Mak	University of Macau, Macau, SAP
Lodge Pun	University of Macau, Macau, SAP
Chulhong Kim	Pohang University of Science and Technology, South Korea
Suparerk Janjarasjitt	Ubon Ratchathani University, Thailand

Preface

The 12th IFMBE Asian Pacific Conference on Medical and Biological Engineering (APCMBE2023) was held in Suzhou, China, from 18 to 21 May 2023. The conference was organized by the Chinese Society of Biomedical Engineering (CSBME) and was endorsed by International Federation for Medical and Biological Engineering (IFMBE).

Aimed to gather talents in the fields of medicine, enterprise, research, and education, APCMBE2023 focused on key fields and key technologies of biomedical engineering and promoted the integration of multiple disciplines. Special attention was paid to the frontiers of biomedical engineering, including medical artificial intelligence, neural engineering, medical imaging, computer-aided surgery, biosensors, rehabilitation engineering, medical informatics, biomechanics, and other hot topics and key issues. The progress of biomedical engineering has provided strong support for the realization of translational medicine and personalized medicine based on interdisciplinary cooperation and information sharing. Improving medical standards and ensuring people's health are a long journey and a highly challenging undertaking. We need to maintain an open, innovative, and cooperative spirit, jointly address the challenges, and promote the continuous progress and transformation of technology in biomedical engineering.

In total, we received 363 contributions, of which 181 contributions were full-length scientific papers, and the rest were short abstract submissions. In total, 100 papers met the standards for publication in the Proceedings of APCMBE2023.

We, the local organizers, would like to thank IFMBE for its support in organizing APCMBE2023. Our thanks go to the members of the International Organizing Committee for their contribution. We extend our thanks to the organizers of topical sessions and the reviewers. They made the creation of these Proceedings possible by devoting their time and expertise to reviewing the received manuscripts and thus allowed us to maintain a high standard in selecting the papers for the Proceedings. And last, but certainly not least, we would like to thank Springer Nature publishing company for the support and assistance in publishing these Proceedings.

Xuetao Cao
President, APCMBE2023

Contents

Computer-Aided Surgery

Inside-Out Accurate Head Tracking with Head-Mounted Augmented Reality Device	3
<i>Haowei Li, Wenqing Yan, Yuxing Yang, Zhe Zhao, Hui Ding, and Guangzhi Wang</i>	
A Model-Guided Method for Ultrasound Probe Calibration	10
<i>Jiasheng Zhao, Haowei Li, Sheng Yang, Chaoye Sui, Hui Ding, and Guangzhi Wang</i>	
Real-Time Medical Tool Runout Monitor Based on Dual Laser Displacement Sensors	18
<i>Sheng Yang, Haowei Li, Hui Ding, and Guangzhi Wang</i>	
Correction of Premature Closure of Sagittal Suture with Small-Incision Traction Bow	26
<i>Shanshan Du, Li Wen, Zhenmin Zhao, and Junchen Wang</i>	
A Home-Style Intelligent Monitoring Sanitize Robot	38
<i>B. Liu, J. Yang, J. Ding, D. Zhao, and J. Wang</i>	
YOLOv7-Based Multiple Surgical Tool Localization and Detection in Laparoscopic Videos	48
<i>Md Foysal Ahmed and Gang He</i>	
A Frequency-Based Analysis Method to Improve Adversarial Robustness of Neural Networks for EEG-Based Brain-Computer Interfaces	56
<i>Sainan Zhang, Jian Wang, and Fang Chen</i>	
Robot-Assisted Optical Coherence Tomography for Automatic Wide-Field Scanning	65
<i>Yangxi Li, Yingwei Fan, and Hongen Liao</i>	
Adversarial Detection and Defense for Medical Ultrasound Images: From a Frequency Perspective	73
<i>Jian Wang, Sainan Zhang, Yanting Xie, Hongen Liao, and Fang Chen</i>	

A Novel Model-Independent Approach for Autonomous Retraction of Soft Tissue 83
Jiaqi Chen, Longfei Ma, Xinran Zhang, and Hongen Liao

A Soft Robot Based on Magnetic-Pneumatic Hybrid Actuation for Complex Environments 91
Zhuxiu Liao, Jiayuan Liu, Longfei Ma, and Hongen Liao

A VR Environment for Cervical Tumor Segmentation Through Three-Dimensional Spatial Interaction 98
Nan Zhang, Tianqi Huang, Jiayuan Liu, Yuqi Ji, Longfei Ma, Xinran Zhang, and Hongen Liao

An Image Fusion Method Combining the Advantages of Dual-Mode Optical Imaging in Endoscopy 106
Shipeng Zhang, Ye Fu, Xinran Zhang, Longfei Ma, Hui Zhang, Tianyu Xie, Zhe Zhao, and Hongen Liao

An End-to-End Spatial-Temporal Transformer Model for Surgical Action Triplet Recognition 114
Xiaoyang Zou, Derong Yu, Rong Tao, and Guoyan Zheng

2D/3D Reconstruction of Patient-Specific Surface Models and Uncertainty Estimation via Posterior Shape Models 121
Wenyuan Sun, Yuyun Zhao, Jihao Liu, and Guoyan Zheng

Semantics-Preserved Domain Adaptation with Target Diverse Perturbation and Test Ensembling for Image Segmentation 128
Xiaoru Gao, Runze Wang, Rong Tao, and Guoyan Zheng

Biomechanics

A New Mathematical Model for Assessment of Bleeding and Thrombotic Risk in Three Different Types of Clinical Ventricular Assist Devices 139
Yuan Li and Zengsheng Chen

Analysis of YAP1 Gene as a Potential Immune-Related Biomarker and Its Relationship with the TAZ Expression 153
Shan He, Rushuang Xu, Qing Luo, and Guanbin Song

Morphological Feature Recognition of Induced ADSCs Based on Deep Learning 167
Ke Yi, Cheng Xu, Guoqing Zhong, Zhiquan Ding, Guolong Zhang, Xiaohui Guan, Meiling Zhong, Guanghui Li, Nan Jiang, and Yuejin Zhang

Micromechanical Properties Investigation of Rabbit Carotid Aneurysms
by Atomic Force Microscopy 176
Guixue Wang, Jingtao Wang, Xiangxiu Wang, Juhui Qiu, and Zhiyi Ye

The Development of the “Lab-In-Shoe” System Based on an Instrumented
Footwear for High-Throughput Analysis of Gait Parameters 183
Ji Huang, Xin Ma, and Wen-Ming Chen

3D-Printed Insole Designs for Enhanced Pressure-Relief in Diabetic Foot
Based on Functionally-Graded Stiffness Properties 192
Xingyu Zhang, Pengfei Chu, Xin Ma, and Wen-Ming Chen

A Novel Force Platform for Assessing Multidimensional Plantar Stresses
in the Diabetic Foot—A Deep Learning-Based Decoupling Approach 200
Hu Luo, Xin Ma, and Wen-Ming Chen

MicroNano Bioengineering

A Nanoparticle Tracking Analysis Algorithm for Particle Size Estimation 211
Song Lang, Yanwei Zhang, Hanqing Zheng, and Yan Gong

Biomaterials

Self-adaptive Dual-Inducible Nanofibers Scaffolds for Tendon-To-Bone
Interface Synchronous Regeneration 221
*A. Haihan Gao, B. Liren Wang, C. Tonghe Zhu, D. Jinzhong Zhao,
and E. Jia Jiang*

Medical Informatics

A Multifunctional Image Processing Tool for CT Data Standardization 243
Yiwei Gao, Jinnan Hu, Peijun Hu, Chao Huang, and Jingsong Li

Effect of Schroth Exercise on Pulmonary Function and Exercise Capacity
in Patients with Severe Adolescent Idiopathic Scoliosis 251
*Wei Liu, Christina Zong-Hao Ma, Chang Liang Luo, Yu Ying Li,
and Hui Dong Wu*

An Imputation Approach to Electronic Medical Records Based on Time
Series and Feature Association 259
Y. F. Yin, Z. W. Yuan, J. X. Yang, and X. J. Bao

A Software Tool for Anomaly Detection and Labeling of Ventilator Waveforms 277
Cheng Chen, Zunliang Wang, Chuang Chen, Xuan Wang, and Songqiao Liu

A Machine Learning Approach for Predicting the Time Point of Achieving a Negative Fluid Balance in Patients with Acute Respiratory Distress Syndrome 284
Haowen Lei, Zunliang Wang, and Songqiao Liu

3D Simulation Model for Urine Detection in Human Bladder by UWB Technology 291
Mengfei Jiang, Liping Qin, Hui Zhen, and Gangmin Ning

AI in Medicine

A Nearest Neighbor Propagation-Based Partial Label Learning Method for Identifying Biotypes of Psychiatric Disorders 301
Yuhui Du, Bo Li, Ju Niu, and Vince D. Calhoun

Predicting Timing of Starting Continuous Renal Replacement Therapy for Critically Ill Patients with Acute Kidney Injury Using LSTM Network Model 309
Chengyuan Li, Zunliang Wang, Lu Niu, and Songqiao Liu

An End-To-End Seizure Prediction Method Using Convolutional Neural Network and Transformer 317
Yiyuan Wang and Wenshan Zhao

Ensemble Feature Selection Method Using Similarity Measurement for EEG-Based Automatic Sleep Staging 325
Desheng Zhang and Wenshan Zhao

Biomedical Photonics

Rapid Virus Detection Using Recombinase Polymerase Amplification Assisted by Computational Amplicon-Complex Spectrum 335
F. Yang, Y. Su, F. G. Li, T. Q. Zhou, X. S. Wang, H. Li, S. L. Zhang, and R. X. Fu

Neuromodulation with Submillimeter Spatial Precision by Optoacoustic Fiber Emitter 343
Ninghui Shao and Hyeon Jeong Lee

Medical Laboratory Engineering

- A Novel Poly(3-hexylthiophene) Microelectrode for Ascorbic Acid Monitoring During Brain Cytotoxic Edema 353
Zexuan Meng, Yuchan Zhang, Lu Yang, Shuang Zhao, Qiang Zhou, Jiajia Chen, Jiuxi Sui, Jian Wang, Lizhong Guo, Luyue Chang, Guixue Wang, and Guangchao Zang

Health Engineering

- Radar Translator: Contactless Eyeblink Detection Assisting Basic Daily Intension Voice for the Paralyzed Aphasia Patient Using Bio-Radar 361
Fugui Qi, Jiani Li, Haoyang Yu, Haoxin Han, Wei Huang, Guohua Lu, and Jianqi Wang
- Image Reconstruction Algorithm in Electrical Impedance Tomography Based on Improved CNN-RBF Model 369
Liyuan Zhang, Xuechao Liu, Lei Li, Feng Fu, Li Jin, and Bin Yang
- An Explainable Assessment for Depression Detection Using Frontal EEG 377
Feifei Chen, Lulu Zhao, Licai Yang, Jianqing Li, and Chengyu Liu
- Heart Murmur Detection in Phonocardiogram Signals Using Support Vector Machines 384
Foli Fan, Yuwei Zhang, Chenxi Yang, Jianqing Li, and Chengyu Liu

Computational Systems, Modeling and Simulation in Medicine, Multiscale Modeling and Synthetic Biology

- SCpipeline: The Tool and Web Service for Identifying Potential Drug Targets Based on Single-Cell RNA Sequencing Data 395
Lu Lin, Qianghan Shao, Xiao Sun, and Hongde Liu
- Study on the Detection of Vertigo Induced by GVS Based on EEG Signal Feature Binary Classification 403
Y. Geng and W. Xue

Therapeutic and Diagnostic Systems and Technologies

- CT Images-Based Automatic Path Planning for Pedicle Screw Placement Incorporating Anatomical and Biomechanical Considerations 421
Xintong Yang, Yunning Wang, Yajun Liu, Xuquan Ji, Anyi Guo, Yan Hu, and Wenyong Liu

Reciprocal Unlocking Between Autoinhibitory CaMKII and Tiam1:
A Simulation Study 429
Zhen Yu, Xiaonian Ji, Jiaqi Zuo, and Xiaodong Liu

Author Index 437

Computer-Aided Surgery



Inside-Out Accurate Head Tracking with Head-Mounted Augmented Reality Device

Haowei Li¹, Wenqing Yan², Yuxing Yang¹, Zhe Zhao^{3,4}, Hui Ding¹,
and Guangzhi Wang¹(✉)

¹ Department of Biomedical Engineering, Tsinghua University, Beijing, China
wgz-dea@tsinghua.edu.cn

² School of Medicine, Tsinghua University, Beijing, China

³ Department of Orthopaedics, Beijing Tsinghua Changgung Hospital, Beijing, China

⁴ School of Clinical Medicine, Tsinghua University, Beijing, China

Abstract. Objective: External Ventricular Drainage (EVD) is a widely used procedure in neurosurgery that is restricted in accuracy and reproducibility due to free-hand operation. Augmented reality (AR) improves punctuation success rate by superimposing virtual paths on the operation area. However, the effectiveness of surgical guidance is affected by tracking accuracy. This paper aims to achieve accurate and stable head tracking during EVD surgery. Methods: We propose a dynamic inside-out tracking method combining retro-reflective markers and point clouds. First, built-in infrared depth sensor of HoloLens 2 is used to identify markers pasted on patient's head for coarse registration of preoperative images and intraoperative patient. Real-time 3D point clouds and point-to-plane ICP registration are then used to further improve tracking accuracy and stability. Meanwhile, we calibrate and correct the depth distortion of the HoloLens 2 depth sensor on different materials, improving the accuracy of point cloud-based tracking methods. Results: The root mean square error (RMSE) of preoperative registration is less than $1.6mm$; average RMSE of intraoperative head tracking is less than $1.28mm$. Meanwhile, average angular tracking jitter is reduced by more than 40% when integrating point clouds. The proposed method can achieve 37.7fps tracking. Conclusion: The retro-reflective marker and point cloud hybrid tracking method in this paper can achieve high-precision real-time head tracking, providing the potential for accurate visual guidance in EVD surgery.

Keywords: Augmented Reality · Head Tracking · Point Cloud · Surface Reconstruction

1 Introduction

EVD surgery is a neurosurgery widely used in acute hydrocephalus, intraventricular hemorrhage and intracranial hypertension [1, 2]. The accuracy of drainage tube insertion affects the probability of brain injury and complications, thus determining the success

Haowei Li and Wenqing Yan have contributed equally to this work.

of the operation. Traditional freehand puncture process uses surface feature points as a reference and strongly relies on the surgeon's experience [3], leading to low accuracy and reproducibility, higher complication probability and higher operative risk. Image-guided operation uses infrared tools for tracking of patients and surgical tool and provides visual guidance on 2D monitors. However, this would lead to complex system setup, distraction of surgeons' attention and hand-eye incoordination [4].

Augmented reality enhances neurosurgery operation accuracy by providing visual guidance as superimposed virtual images [5]. A core problem during this procedure is to track patient accurately with AR device. Liebmann et al. used a pointer with AprilTag for spine surface digitalization [6], and then used point cloud registration method for spine tracking. However, the tracking accuracy is restricted by the marker size and point cloud sparsity. Kunz et al. used infrared depth sensor of HoloLens for retro-reflective marker tracking [7], reaching submillimeter translation error, which is then proven to behave relatively poorly on angular error [8]. Point cloud registration has been used for marker-less tracking, which can potentially provide more stable results. However, Gu et al. proved that a systematic depth error exists on the infrared depth sensor integrated on commercial AR devices [9], leading to large tracking errors.

To provide accurate and stable tracking results in EVD, this work proposes a method integrating retro-reflective marker tracking and point cloud registration for real-time accurate head tracking. A calibration and correction procedure is first finished for HoloLens 2 depth sensor on different materials. A surface reconstruction procedure is then proposed for accurate preoperative marker-patient registration. Finally, marker tracking and point cloud registration are used in sequence to provide real-time stable tracking.

2 Methods

This paper proposes a method that only uses built-in depth sensor in HoloLens 2 to enable accurate and stable head tracking by combining infrared retro-reflective markers and point clouds (Fig. 1). To provide a larger field of view and higher resolution, the Articulated Hand Tracking (AHAT) mode of HoloLens 2 depth sensor [10] is used to acquire data for both markers and point clouds. To take advantage of both methods, retro-reflective markers are pasted on the patient's head and registered with preoperative images. Intraoperatively, markers are used to provide coarse tracking results; point clouds are then used for pose enhancement. This section details the framework of the method, including tool definition and detection, depth camera undistortion, preoperative registration and dynamic head tracking. To prove the capability of our method, we conducted a series of experiments on preoperative registration, intraoperative tracking and efficiency.

2.1 Retro-reflective Tool Definition and Detection

Retro-reflective tapes are cut into circles and pasted on the patients' heads ($n \geq 3$) to provide coarse tracking results. A procedure including marker detection, tool definition and tool detection is then used for coarse tracking. During marker detection, 2D

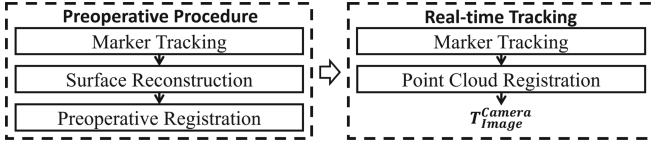


Fig. 1. Proposed EVD intraoperative head tracking framework.

marker centers are first recognized from the image with threshold criterion and connected component detection. Providing camera intrinsic parameters and depth values, marker positions in camera space C can be calculated as $X_i = d_i(x_i, y_i, 1)^T / \|(x_i, y_i, 1)\|_2$. Given a specific tool shape A , the difference between it and a marker frame can be evaluated with rigid body fitting error. The geometric mean of this error on multiple frames is then used as the target for tool shape optimization. Finally, distance information between different markers in a frame and the tool definition is used to recognize the tool from sensor data and is then used to calculate the tool pose T_A^C .

2.2 Camera Depth Undistortion

In the work of Gu et al. [9], a systematic depth error is proved to exist in AHAT camera, which would bring large error to point cloud based tracking method. Meanwhile, due to different textures, colors and other surface characteristics, different materials may present different errors. In order to achieve higher tracking accuracy, a calibration and undistortion procedure is completed on four materials including nylon, photopolymer, PC-ABS and PLA. As retro-reflective tracking method is proved to present a low systematic error, it is regarded as reference material during calibration.

As shown in Fig. 2a, a structure was designed to keep all materials on one plane. The structure was fixed at different depths and angles. Each time, 250 frames of sensor data were collected. The standard errors of the depth over 250 frames were used to describe the depth stability. Point clouds from the reference material were used to fit a reference plane, and depth error δ of a certain point was calculated as the distance from the point to the reference plane along the depth direction. First, a single point cloud showed that different materials behaved differently in both error and stability (Fig. 2b). In the depth stability test, depth values on retro-reflective material were proved to be more stable than those on other materials ($p < 0.5$). In terms of depth error, a significant difference was revealed between any two different materials at all depths and angles ($p < 0.5$), while single material was also proved to present differently at different depths or angles ($p < 0.5$). To undistort the depth value, the average depth error at 15 different depths from 382 mm to 655 mm was used to represent the systematic depth error of a certain material. As a result, nylon, PLA, photopolymer and PC-ABS respectively presented a depth error of 11.04mm, 25.79 mm, 23.91 mm and -6.63 mm.

2.3 Preoperative Registration

During preoperative registration, multiple frames of sensor data are used to register retro-reflective markers and medical images. The tool shape A is first optimized, which

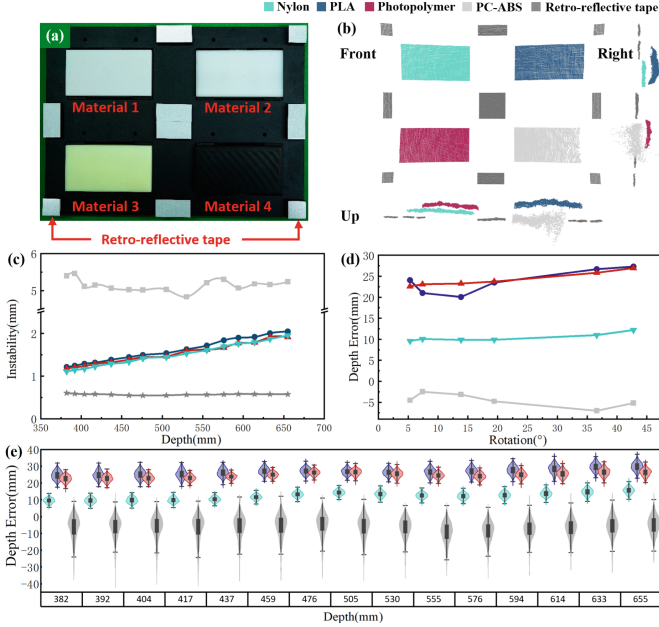


Fig. 2. **a** Structure for AHAT depth calibration. **b** Single frame point cloud of the calibration structure at different views. **c** Instability of the depth value at different depths. **d, e** Depth value error of different materials at different angles and depths.

is then used to calculate the relative pose between markers and AHAT camera in each frame. Depth values from the sensor are then corrected according to the target material as $d_i^i = d_i - \delta$. Then, GPU-based TSDF [11] reconstruction is processed for head surface. By registering this surface and extracted surface from images with point-to-plane ICP algorithm, the spatial transformation from preoperative image to the retro-reflective markers can be calculated as T_I^A .

2.4 Dynamic Head Tracking

Retro-reflective marker tracking stability is limited by depth data quality and is relatively unstable in rotation. To utilize both the speed of marker tracking and stability of point cloud registration, markers are used for coarse tracking result as $T_{I,coarse}^C = T_A^C T_I^A$ first. Point-to-plane point cloud registration is further used to refine the pose and get final tracking result as $T_{I,fine}^C$.

3 Experiments and Results

3.1 Preoperative Registration

In order to test the precision of preoperative registration, a head phantom was 3D printed with nylon. In each group, 3, 4, 5 or 6 markers were stucked on the phantom and 1200 frames of sensor data were recorded for surface reconstruction and registration. As

shown in Fig. 3a, b, reconstructed surface provided more details and was smoother. RMSE of preoperative registration was smaller and the inlier point rate was higher when depth distortion was considered (Fig. 3f, g). When three markers were used, an RMSE less than 1.6mm was presented. Meanwhile, registration error tended to decrease when marker number increased, which may due to more stable tool poses provided by increased markers. Moreover, another experiment was conducted to reconstruct more complete phantom surface with the guiding of 9 markers (Fig. 3e). The result showed that the reconstructed surface fit the real model surface better when we considered depth distortion, and a large systematic error would exist in point cloud-based tracking method when this distortion was neglected due to the large gap between the reconstructed surface and ground-truth (GT).

3.2 Tracking Stability

To evaluate the effect brought by adding point cloud registration, another 1200 frames were collected when HoloLens 2 and phantom kept static. Tracking results were calculated from both retro-reflective marker tracking and the proposed method. Tracking RMSEs and angular differences between frames were then calculated for evaluation. As shown in Fig. 3h, i, proposed method presented more stable than retro-reflective markers in angular tracking under all conditions. The mean angular jitter was 0.61 mm when 3 markers were used for tracking. A decrease of more than 40% was found on mean angular tracking jitter intensity on all marker numbers. However, proposed method presented higher mean tracking RMSEs (1.28mm at max), which may be due to higher depth instability on nylon material compared to retro-reflective tapes.

3.3 System Performance

The performance of the proposed method was further tested on Intel 13900K CPU and RTX 4090 GPU.

Preoperative reconstruction and dynamic tracking respectively reached 217.4*fps* and 37.7*fps*. Therefore, a potential of real-time tracking is proven.

4 Discussions

This paper proposes a method for inside-out accurate and stable head tracking during EVD surgery using infrared depth sensor. According to our experiments, retro-reflective materials presented more stable than other materials, which may ensure a relatively accurate pose when marker number was limited. Meanwhile, different materials were found to have different systematic depth errors compared to retro-reflective materials. The mean error under 15 different depths were used to correct the depth images. The reconstruction test showed that depth information after depth correction fit GT better (Fig. 3e). Preoperative registration showed an error less than 1.6mm and an inlier point rate higher than 99.8%, demonstrating a high accordance between reconstructed surface and GT. A mean RMSE less than 1.5mm was found during dynamic tracking. It was also proved that the proposed method could decrease angular jitter by more than 40%, thus

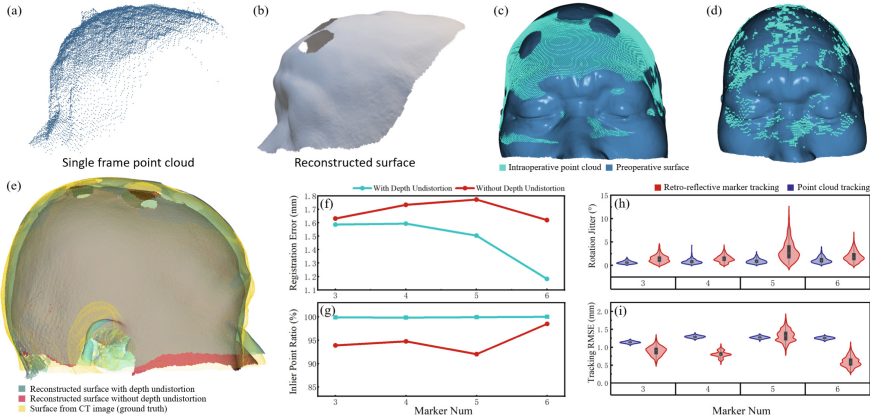


Fig. 3. **a** A frame of point cloud from AHAT camera. **b** Reconstructed head surface. **c** Preoperative registration result of reconstructed head surface and image. **d** Intraoperative registration result of single frame point cloud and image. **e** Comparison of reconstructed surface with and without depth undistortion. **f, g** Registration RMSE and inlier point ratio of reconstructed surface and surface from CT image. **h, i** Angular tracking jitter and RMSE of two different tracking methods under different retro-reflective marker quantities.

could potentially provide more accurate tracking result during EVD surgery. Finally, the performance test showed that the method could run at more than 37fps during dynamic tracking.

Comparatively, our method mainly contributes in:

1. Undistort depth error for AR built-in sensor, increasing tracking accuracy of point cloud-based tracking method.
2. Propose a method for high resolution smooth surface reconstruction with built-in AR sensor.
3. Integrate infrared markers and point clouds for more accurate and stable tracking.

Despite promising tracking stability and accuracy presented by proposed method, certain limitations exist. Mean depth error on 15 different depths was used to correct depth images. However, it was proved that different depth errors existed when depths and angles were different, which led to local distortion during reconstruction (Fig. 3e). Meanwhile, different materials have different depth errors, and complex scenarios where surfaces of multiple materials need to be reconstructed simultaneously may be difficult. Therefore, more studies are needed to better calibrate and correct the depth error before it can provide more accurate information.

5 Conclusions

This paper proposes an inside-out head tracking method that uses built-in depth sensor in head-mounted mixed reality device, integrating retro-reflective marker detection and point cloud registration. The method enables stable and real-time head tracking without

additional electronics, fixed rigid tracking tools or prior tool shape information. The proposed method showed a registration error of $RMSE < 1.6\text{mm}$ during preoperative procedure. It is also proved that the method can decrease the intraoperative angular tracking jitter by over 40%. Therefore, the proposed tracking method can potentially provide stable and accurate real-time tracking information for visual guidance in EVD surgery.

Acknowledgments. This study is supported by NSFC (U20A20389), National Key R&D Program of China (2022YFC2405304), Tsinghua University Clinical Medicine Development Fund (10001020508) and Tsinghua ISRP (20197010009).

References

1. Srinivasan, V.M., O'Neill, B.R., Jho, D., et al.: The history of external ventricular drainage: Historical vignette. *J. Neurosurg.* **120**(1), 228–236 (2014)
2. Kakarla, U.K., Kim, L.J., Chang, S.W. et al.: Safety and accuracy of bedside external ventricular drain placement. *Neurosurgery* **63**(1 Suppl_1), ONS162-ONS167 (2008)
3. Pelargos, P.E., Nagasawa, D.T., Lagman, C., et al.: Utilizing virtual and augmented reality for educational and clinical enhancements in neurosurgery. *J. Clin. Neurosci.* **35**, 1–4 (2017)
4. Fried, H.I., Nathan, B.R., Rowe, A.S., et al.: The insertion and management of external ventricular drains: an evidence-based consensus statement. *Neurocrit. Care.* **24**(1), 61–81 (2016)
5. Meola, A., Cutolo, F., Carbone, M., et al.: Augmented reality in neurosurgery: a systematic review. *Neurosurg. Rev.* **40**(4), 537–548 (2017)
6. Liebmann, F., Roner, S., von Atzigen, M., et al.: Pedicle screw navigation using surface digitization on the Microsoft HoloLens. *Int. J. Comput. Assist. Radiol. Surg.* **14**(7), 1157–1165 (2019)
7. Kunz, C., Maurer, P., Kees, F. et al.: Infrared marker tracking with the HoloLens for neurosurgical interventions. *Curr. Dir. Biomed. Eng.* **6**(1) (2020)
8. Martin-Gomez, A., Li, H.W., Song, T.Y., et al.: STTAR: surgical tool tracking using off-the-shelf augmented reality head-mounted displays. *IEEE Trans. Vis. Comput. GR* (2023). <https://doi.org/10.1109/TVCG.2023.3238309>
9. Gu, W.H., Shah, K.J., Knopf, J., et al.: Feasibility of image-based augmented reality guidance of total shoulder arthroplasty using microsoft HoloLens 1. *Comput. Meth. Biomech. Biomed. Eng. Imaging Vis.* **9**(3), 261–270 (2021)
10. Ungureanu, D., Bogo, F., Galliani, S. et al.: Hololens 2 research mode as a tool for computer vision research (2020). [arXiv:2008.11239](https://arxiv.org/abs/2008.11239)
11. Curless, B., Levoy, M.: A volumetric method for building complex models from range images, *ACM. Proc. Annu. Conf. Comput. Graph. Interact. Tech.* New Orleans, LA, USA **1996**, 303–312 (1996)



A Model-Guided Method for Ultrasound Probe Calibration

Jiasheng Zhao, Haowei Li, Sheng Yang, Chaoye Sui, Hui Ding,
and Guangzhi Wang^(✉)

Department of Biomedical Engineering, Tsinghua University, Beijing, China
wgz-dea@tsinghua.edu.cn

Abstract. Objective: Ultrasound (US) probe calibration is critical for the localized ultrasound system. Key points and surfaces are often used for calibration, whose accuracy is restricted by the ultrasound volume effect. The aim of this paper is to accurately calibrate the US probe under volume effect. Method: We present a model-guided ultrasound probe calibration method, to provide accurate calibration results under volume effect. First, we design a rotationally symmetric calibration phantom unit to provide image areas weekly affected by volume effect during continuous scanning. Second, US images from the uncalibrated probe are used to reconstruct the 3D image volume. Finally, we use image registration and point registration for super-resolution unification of US images, the model and the tracking device. Results: In multiple probe calibration experiments at different probe depths, the average calibration precision was 0.163 mm; in the needle tip tracking experiment, the average detection accuracy was 0.335 mm. Conclusion: Guided by the specially designed model, our method can realize precise and accurate ultrasound probe calibration under volume effect.

Keywords: Ultrasound probe calibration · Volume effect · Model-guided · 3D reconstruction

1 Introduction

Localized ultrasound systems combine ultrasound probe with tracking devices (e.g., optical tracker, magnetic tracker, end of a robot arm), to provide spatial information. This combination endows temporally advantaged ultrasound spatial information and extends the application scenarios. In previous studies, localized ultrasound systems have been used to provide quantitative spatial information for ultrasound-guided punctuations [1, 2] and 3D reconstructions [3–5].

Accurate US probe calibration is critical for correct positions of US images. Existing calibration methods often use positions of key points and lines in tracking space and image space. However, US images represent the accumulation of reflection signals within an area, leading to the volume effect which would generate artifacts near the key features and reduce the calibration accuracy.

Prager et al. [6] used a mechanical device to keep US probe perpendicular to the calibration plane, in order to ensure the correct position it presents in US images. This

method requires a complex setup. Chen et al. [7] calculated the thickness of the acoustic beam based on the artifact distribution and used it to eliminate further the error caused by volume effects. However, this method is time-consuming and prone to human mistakes. N-line phantom is widely used in US probe calibration. Researchers [8, 9] have used various image-processing algorithms to automatically extract the intersection positions of the phantom and US image planes from images including volume artifacts. Wang et al. [10] integrated spatial position from line phantoms and geometric features from the model’s surface for higher calibration accuracy. However, this method is still proven to be influenced strongly by the volume effect.

To realize accurate US probe calibration under volume effect, we propose a model-guided calibration method that can take advantage of the artifact’s shape. First, a model structure is designed to obtain image areas weakly affected by the volume effect during continuous scanning. US 3D reconstruction is then used for model reconstruction with an uncalibrated US probe. After that, the 3D image is registered with the model surface for super-resolution locations of key features. Finally, the model is used to connect the phantom and US image to realize accurate calibration.

2 Methods

2.1 Calibration Model Design and General Ideas

The ultrasound volume effect expands the key features of the target which are not perpendicular to the image plane and blurs the image. This phenomenon affects the precision of the extraction of key features, thus reducing US probe calibration accuracy. Meanwhile, surfaces with different slopes have different volume artifact areas. Therefore, we propose a rotationally symmetrical calibration unit with continuously varying slopes. A rotationally specific calibration structure is then designed with multiple calibration units (Fig. 1a).

As shown in Fig. 1b, during the continuous US scanning of the calibration unit, the area of the artifact caused by the volume effect changes with the angle between the US image and phantom surface. Generally, the artifact width in the normal direction of the edge increases when the probe moves from the center of the calibration unit to the margin. The artifact caused by the volume effect is minimal when the US plane passes through the center line of the calibration unit.

Based on these features, we register the artifact-free model surface to 3D reconstructed US image to realize super-resolution US feature extraction. The complete working flow is shown in Fig. 2. The model is respectively registered with the reconstructed US image and the phantom, and is used as the bridge between the ultrasound image and the phantom for accurate calibration.

2.2 3D Reconstruction Based on an Uncalibrated Probe

A 6 degree of freedom tracking target M is rigidly fixed on the US probe and an external tracking device W is used to track the probe and give the pose of the target as $T_M^W = (R_M^W, t_M^W)$. The US reconstruction is then finished by calculating the position of every pixel in the space W in each frame.

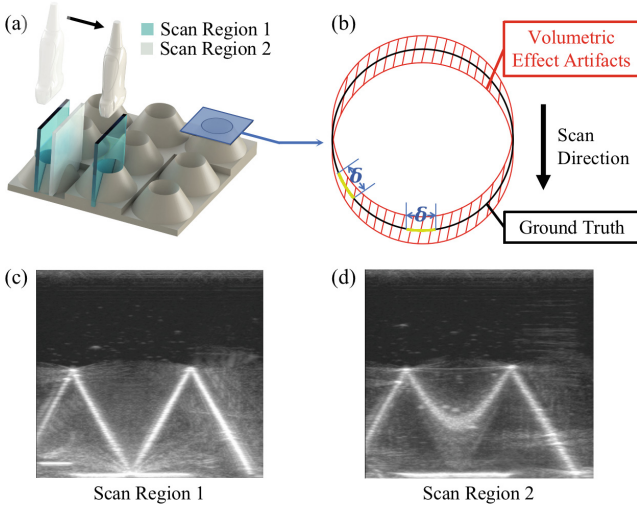


Fig. 1. **a** Calibration phantom containing $3 * 3$ basic units. **b** The areas influenced by volume effect in a cross-section. **c** Image acquired at the centerline of the calibration unit. **d** Image acquired at other locations.

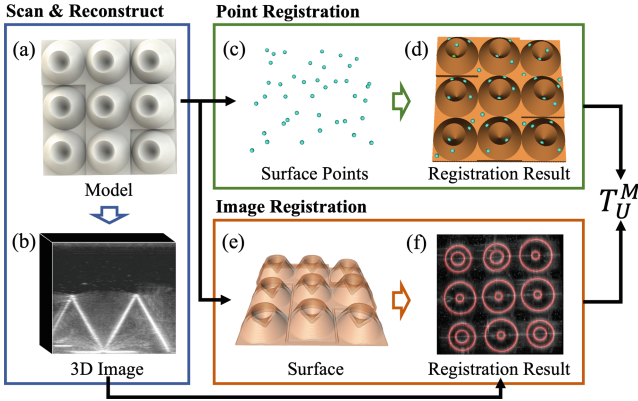


Fig. 2. System working flow: **a** Calibration model. **b** Reconstructed 3D ultrasound image. **c** Points picked from the phantom. **d** Registration results of the points and the phantom. **e** The surface extracted from the model. **f** Registration result of the model surface and US image.

Giving the pixel spacing (s_x, s_y) of US image, the position of pixel (u_i, v_i) in US probe coordinate system U can be calculated as $X_i = (u_i s_x, v_i s_y, 0)^T$. Therefore, the position of the i th pixel and the j th frame in space W can be represented as:

$$t_{i,j}^W = R_{M,j}^W (R_U^M X_{i,j} + t_U^M) + t_{M,j}^W \quad (1)$$

where (R_U^M, t_U^M) is the spatial transformation between the US probe and the tracking target. Moreover, R_U^M can be directly determined by the assembly structure.

For an uncalibrated US probe, we designed a value $f_{i,j}^W$, which has a similar form compared to $t_{i,j}^W$:

$$f_{i,j}^W = R_{M,j}^W \left(R_U^M X_{i,j} \right) + t_{M,j}^W \quad (2)$$

Using the properties of rigid spatial transformations, the difference between $t_{i,j}^W$ and $f_{i,j}^W$ can be calculated:

$$t_{i,j}^W - f_{i,j}^W = R_{M,j}^W t_U^M \quad (3)$$

For a scanning process where the rotation of the US probe $R_{M,j}^W$ has not changed, the displacement of any pixel between the real 3D position and that calculated with $f_{i,j}^W$ remains constant. Thus, we define a space W' based on $f_{i,j}^W$, which only differs from space W on translation: $t_{W'}^W = R_M^W t_U^M$. By converting pixels in every frame to space W' , we can reconstruct US image without probe calibration.

To acquire US images where rotation is fixed, the probe is fixed on a robot arm for translational movement. After acquiring a series of US 2D images I_j , 3D spatial positions of these points are calculated using Eq. (2) to form point clouds $\{P_j\}$ with intensity information. After that, voxel down sampling and Gaussian filtering are used to generate the 3D reconstructed US image I^{3D} (Fig. 2b).

2.3 Image Registration

To provide super-resolution information for probe calibration, this section registers the model space I to US reconstruction space W' under volume effect using reconstructed image I^{3D} and the outer surface from the designed model.

In the cross-sectional direction (Fig. 1b), during the scanning procedure where the probe rotation is fixed, the width of the artifact caused by the volume effect is the smallest when the US image crosses the centerline of the calibration unit, and increases when the probe moves to the margin. Meanwhile, the intensity of US images near the true surface is higher and decreases on both sides (Fig. 1d). The intensity outside the artifact area can be regarded as 0.

Based on such volume artifact features, we first extract the outer surface of the model with morphological processing (Fig. 2e) and rigidly register the surface to the reconstructed image I^{3D} based on Mattes mutual information [11, 12]. When the model surface is not completely aligned with the real surface in the US image, some areas of the model surface would be in the low-intensity artifact region or outside the artifact region of the US image, thus the error of similarity measurement would increase. When they are perfectly aligned, the error of similarity measurement would reach the minimum. Therefore, the relationship $T_I^{W'}$ between the model space I and the space W' can be obtained by optimizing the Mattes mutual information values through stepwise iterations. At the same time, the size of the volume artifact varies at different depths of the probe, so the 3D rigid registration can take advantage of the global volume artifact properties to improve the registration accuracy.

For practical implementation, we use the model surface with a certain thickness for registration to address the effects of voxelization of the model surface, US image resolution and the multiple noises in real US.

2.4 Probe Calibration

To finally calibrate the US probe, this section first registers the model space I to tracking device W . A tracking probe is first used for the coordinates localization of the conical tips, with which a coarse registration result $T_{I,coarse}^W$ can be calculated. After that, the tracking probe is further used to fetch surface points on the model. Using $T_{I,coarse}^W$ for initiation and the geometric mean of the minimum Euclidean distances from the fetched points to the model for evaluation, an iterative optimization method is used to obtain the transformation from the model to the tracking device T_I^W (Fig. 2d).

Finally, the transform between tracking device W and the space W' can be calculated as $T_{W'}^W = T_I^W (T_I^{W'})^{-1}$, and the US probe calibration result t_U^M can therefore be calculated:

$$t_U^M = (R_M^W)^{-1} t_{W'}^W, \quad (4)$$

3 Experiments and Results

To verify the performance of the ultrasound probe calibration method proposed in this paper, we fabricated the designed calibration phantom using the stereolithography 3D printing method with resin. The model was placed in a water tank which was kept at 37 °C constantly to simulate sound speed in the human body [9]. The localized ultrasound systems included a 2D ultrasound system (Mindray DC8 with probe L12-3E), a magnetic tracking device (Northern Digital Incorporated Aurora®), and a graphics computing server (Intel® Core™ i9-10900X CPU @ 3.70GHz × 20, Ubuntu 20.04.5 LTS). The ultrasound image is acquired in the graphics server via a video capture card. To resolve the time asynchrony between the ultrasound image and the tracking information from different devices, we use a plane imaging and periodic motion based method [9] for time calibration. The time delay was tested to be approximately 106 ms.

In this section, the precision of the calibration results was first verified. Four sets of calibration experiments were conducted at probe depths of 30 mm, 35 mm, and 40 mm respectively, and the root mean square error (RMSE) of calibration results on translation was calculated on each axis to evaluate the calibration precision. The results are shown in Table 1, where the precision ranges from 0.14 mm to 0.19 mm.

After the calibration procedure, feature point picking-up errors were used to evaluate the accuracy of calibration results. A wooden needle tip was used as the test target. A magnetic tracking probe was used to pick the tip position 10 times, whose mean value was used as the experiment's ground truth (GT). The positions of the needle tips were extracted from the US images at each probe depth, and the 3D spatial positions were then calculated based on the calibration results. The standard deviation of the picked points